

Structural anomalies associated with the electronic and spin transitions in LnCoO_3 .

K. Knížek, Z. Jirák, J. Hejtmánek, M. Veverka, and M. Maryško

Institute of Physics ASCR, Cukrovarnická 10, 162 53 Prague 6, Czech Republic.

G. Maris and T. T. M. Palstra

Solid State Chemistry Laboratory, Materials Science Centre,

University of Groningen, Nijenborg 4,

9747 AG Groningen, The Netherlands

Abstract

A powder X-ray diffraction study, combined with the magnetic susceptibility and electric transport measurements, was performed on a series of LnCoO_3 perovskites ($\text{Ln} = \text{Y, Dy, Gd, Sm, Nd, Pr and La}$) over a temperature range 100 - 1000 K. A non-standard temperature dependence of the observed thermal expansion was modelled as a sum of three contributions: (1) Weighted sum of lattice expansions of the cobaltite in the diamagnetic low spin state and in the intermediate (IS) or high (HS) spin state. (2) An anomalous expansion due to the increasing population of excited (IS or HS) states of Co^{3+} ions at the course of the diamagnetic-paramagnetic transition. (3) An anomalous expansion due to excitations of Co^{3+} ions to another paramagnetic state accompanied by an insulator-metal transition.

The anomalous expansion is governed by parameters that are found to vary linearly with the Ln ionic radius. In the case of the first magnetic transition it is the energy splitting Δ between the ground low spin state and the excited state, presumably the intermediate spin state. The energy splitting Δ , determined by a fit of magnetic susceptibility, decreases with temperature. The values of Δ determined for LaCoO_3 and YCoO_3 at $T = 0$ K as 164 K and 2875 K, respectively, fall to zero at $T = 230$ K for LaCoO_3 and 860 K for YCoO_3 . The second anomalous expansion connected with a simultaneous magnetic and insulator-metal transition is characterized by its center at $T = 535$ K for LaCoO_3 and 800 K for YCoO_3 . The change of the unit cell volume during each transition is independent on the Ln cation and is about 1% in both cases.

PACS numbers: 61.10.Nz; 71.30.+h.

Keywords: Thermal expansion, spin-state transition, insulator-metal transition, rare-earth perovskite cobaltites.

I. INTRODUCTION

The magnetic and electric transport properties of rare-earth cobalt perovskites LnCoO_3 ($\text{Ln} = \text{La, Y, rare-earth}$) were most detailed studied on LaCoO_3 . At low temperatures LaCoO_3 is nonmagnetic, Co^{3+} ion being in the LS state with six electrons in the t_{2g} levels and empty e_g states (LS, $t_{2g}^6 e_g^0$, $S = 0$). At 50 - 100 K LaCoO_3 undergoes a transition to a magnetic state, the character of which is still under intense debate. Its origin is in a thermal population of excited Co^{3+} states that are either of the intermediate spin (IS, $t_{2g}^5 e_g^1$, $S = 1$) or the high spin (HS, $t_{2g}^4 e_g^2$, $S = 2$) character. A second transition at 500 - 550 K is of an insulator-metal (I-M) kind and is accompanied by a further change of paramagnetic properties.

The analogous compound YCoO_3 also undergoes diamagnetic-paramagnetic transition but more diffusive and shifted to higher temperatures between 450 and 800 K [1]. The I-M transition occurs around 750 K.

The temperatures of the magnetic transitions of the other LnCoO_3 perovskites are difficult to determine by magnetic susceptibility measurement due to the large magnetic moment of the rare-earth element, which masks a possible change of the magnetic state of cobalt. However, recently Yan *et al.* [2] disclosed the magnetic transitions of PrCoO_3 and NdCoO_3 by subtracting a magnetic susceptibility of the corresponding LnAlO_3 . They determined that the excitation to IS or HS states begins at 35 K, 200 K and 300 K for LaCoO_3 , PrCoO_3 and NdCoO_3 , respectively. Alternatively, information on the spin state transition was deduced from a temperature dependent infrared spectroscopy [3]. The spectra of LnCoO_3 single-crystals revealed anomalies in LaCoO_3 , PrCoO_3 and NdCoO_3 around 120, 220 and 275 K, respectively. At these temperatures a decrease of the intensities of stretching and bending modes associated with the LS state was observed, which was accompanied by an increase of new bands ascribed to the IS state.

As to the I-M transitions in the LnCoO_3 series, the published resistivity data evidence a clear correlation with the ionic radius of Ln cations. The transition temperature, defined as the maximum in activation energy of electrical resistivity, thus increases systematically and is shifted from 500 K for LaCoO_3 to 650 K for GdCoO_3 [4] and 750 K for YCoO_3 [1].

The magnetic and electronic transitions are accompanied also by subtle changes in the crystal structure, which is of the rhombohedral perovskite type $R\bar{3}c$ for LaCoO_3 and the

orthorhombic *Pbnm* type for the other LnCoO_3 with smaller rare-earth or yttrium cations. The effects are of two kinds. First, the ionic radius of Co^{3+} increases from $r_{LS} = 0.545 \text{ \AA}$ to $r_{IS} = 0.56 \text{ \AA}$ or $r_{HS} = 0.61 \text{ \AA}$ [5]. Second, Co^{3+} ion in IS or HS state is Jahn-Teller active and corresponding distortion of CoO_6 octahedra may arise. In particular, a monoclinic distortion of the LaCoO_3 structure (space group *I2/a*) and Jahn-Teller distortion of CoO_6 octahedra was found recently by single-crystal X-ray diffraction between 100 and 300 K [6].

The Co^{3+} size effect is responsible for an anomalous thermal expansion that reflects the increasing population of magnetic species. This was indeed observed for LaCoO_3 on single-crystal material around 50 K by dilatometry [7] and neutron scattering [8] and by powder neutron diffraction both around 50 K and second magnetic transition at 500 - 550 K [5, 9]. High temperature X-ray diffraction revealed anomalous thermal expansion also for other LnCoO_3 , namely $\text{Ln} = \text{Nd}, \text{Gd}, \text{Dy}$ and Ho [10] and YCoO_3 and LuCoO_3 [11]. The characteristic temperatures of the structural anomalies shift to higher temperature with decreasing Ln ionic radius. Simultaneously, the onset of magnetic transition is shifted to ≈ 440 K for YCoO_3 and to ≈ 540 K for LuCoO_3 [11].

This paper reports on the structural and electric transport investigation of the LnCoO_3 series over a wide temperature range 100 - 1000 K. Our aim was to resolve different contributions to the thermal expansion in order to establish a quantitative basis for the interrelation of thermal anomalies with the electronic and spin-state transitions.

II. EXPERIMENTAL

Samples of YCoO_3 , DyCoO_3 , GdCoO_3 , SmCoO_3 , NdCoO_3 , PrCoO_3 and LaCoO_3 were prepared by a solid state reaction from stoichiometric amounts of $\text{Co}(\text{NO}_3)_2 \cdot 6\text{H}_2\text{O}$ and respective oxides Y_2O_3 , Dy_2O_3 , Gd_2O_3 , Sm_2O_3 , Nd_2O_3 , Pr_6O_{11} and La_2O_3 . The mixtures were first heated at 600°C to remove nitrate. Resulting powder was pressed in the form of pellets and sintered at 900°C (Y), 1000°C (Dy, Gd, Sm, Nd and Pr) or 1200°C (La) for 100 hours under oxygen flow.

X-ray diffraction confirmed single-phase character of the samples, except for YCoO_3 , where about 2% of Y_2O_3 was detected in agreement with previous observations [12].

The temperature depending structural characterization over the range 100 - 1000 K was performed using the X-ray powder diffractometer Bruker D8 (CuK α , energy dispersive SOL-

X detector) equipped with a MRI TC-wide range temperature chamber. The measurements were performed under ambient atmosphere. Two scans were measured for each temperature and the measured intensities compared in order to check, whether the sample had not changed during the measurement of one temperature. The X-ray diffraction patterns were evaluated by Rietveld profile analysis using the FULLPROF program (version Mar98-LLB JRC).

Measurements of the electrical resistivity and thermoelectric power over the range 290 - 1000 K were done in a small tubular furnace with precisely controlled temperature. The standard K-type thermocouples (chromel - alumel) were used for monitoring of the sweeping temperature gradient ± 5 K imposed across the sample by means of an additional heater. The voltage drop associated with thermal gradient was measured using chromel wires of the K-type thermocouple and chromel thermoelectric power was subtracted (based on Omega standard tables). The four-point steady state method for the electrical resistivity was applied.

The magnetic susceptibility of the LaCoO_3 and YCoO_3 compounds was measured on a SQUID magnetometer up to 400 K using a DC field 100 Oe and subsequently using 10 kOe in order to saturate the effect of small ferromagnetic impurity in the essentially diamagnetic phases (see also [13]). The high temperature data up to 900 K were obtained using a compensated pendulum system MANICS in a field 19 kOe.

Thermogravimetric analysis (TGA) was performed in order to exclude the possible influence of changing oxygen stoichiometry. The TGA was measured using a 2960 SDT of TA Instruments using typically 50 mg sample in Pt pans. Corrections were made for the empty sample holder response. TGA was measured in air, under the same condition as HT-XRD, in the temperature range 573 - 1073 K. The maximum measured change of oxygen stoichiometry was found to be less than 0.1 mol%, *i.e.* below $\gamma = 0.003$ according to formula $\text{LnCoO}_{3-\gamma}$.

III. RESULTS AND DISCUSSION

The lattice parameters at room temperature of the $Pbnm$ compounds are plotted in Fig. 1 in dependence on the respective Ln^{3+} ionic radii (9-fold coordination). The observed values agree with other literature data [14]. Let us remind the Goldschmidt tolerance factor, which

is a fundamental parameter determining the kind of structural distortion in perovskites with the general formula ABO_3 . It is defined as

$$t = \frac{r_A + r_O}{\sqrt{2}(r_B + r_O)} \quad (1)$$

where r_A , r_B and r_O are ionic radii of the respective cations and oxygen. The relation $b > c/\sqrt{2} > a$ observed from YCoO_3 to SmCoO_3 ($t < 0.92$) is typical for structures of so-called O-type, where buckling of the octahedra network is the dominating source of the orthorhombic distortion. The buckling is becoming smaller with increasing size of the rare-earth cation and this effect is manifested by the linearly increasing average Co-O-Co bond angle, see the inset of Fig. 1. For NdCoO_3 and PrCoO_3 ($r_{Ln} > 1.15 \text{ \AA}$, $t > 0.92$) a small local distortion of the CoO_6 octahedra, namely deviation of the O-Co-O angle from 90° (common for orthoperovskites), starts to prevail over the buckling. As a consequence the relation of lattice parameters changes to $a > c/\sqrt{2} > b$.

Displayed in Fig. 1 is also an orthorhombic distortion, which is defined as a standard deviation divided by an average of the lattice parameters

$$dist_{orth} = \frac{\sqrt{\sum (a_i - \bar{a})^2}}{\bar{a}} \quad (2)$$

where $a_i = a$, b and $c/\sqrt{2}$ and \bar{a} is the average of a_i . The orthorhombic distortion decreases linearly in the $b > c/\sqrt{2} > a$ region down to $r_{Ln} = 1.15 \text{ \AA}$, where lattice parameters cross. In the $a > c/\sqrt{2} > b$ region it linearly increases, however with $\approx 3 \times$ smaller slope in absolute value.

No change of the crystal symmetry of the orthorhombic compounds was observed over the experimental temperature range, thus all the diffraction patterns were refined within the same $Pbnm$ space group. The temperature evolution of lattice parameters of the $Pbnm$ compounds is displayed in Figs. 2 and 3. Since the first anomaly in thermal expansion of the rhombohedral LaCoO_3 is outside our experimental range, for this compound we used neutron diffraction data from [5].

For YCoO_3 , DyCoO_3 , GdCoO_3 and SmCoO_3 the relation $b > c/\sqrt{2} > a$ holds for all temperatures. Anomalous thermal expansion is manifested by a rapid S-shaped increase of the b lattice parameter, in agreement with previous reports [10, 11]. This anomaly gives rise to a pronounced minimum in the temperature dependence of the orthorhombic distortion. Its position shifts to lower temperatures with increasing rare-earth ionic radius

r_{Ln} from ≈ 600 K for YCoO_3 to ≈ 400 K for SmCoO_3 . The temperature evolution of lattice parameters below this minimum reflects a higher thermal expansion of ionic $\text{Ln}-\text{O}$ bonds compared to more covalent $\text{Co}-\text{O}$ bonds. Consequently, the tolerance factor t increases with temperature and the orthorhombic distortion decreases with increasing temperature, resembling the room temperature dependence with increasing Ln ionic radius in Fig. 1. On the other hand, the increase of orthorhombic distortion at high temperatures can be related to a gradual increase of $\text{Co}-\text{O}$ bond lengths due to the spin-state transition of Co^{3+} ions, which is responsible for an anomalous decrease of t with temperature and has thus a similar effect as the decrease of r_{Ln} in Fig. 1.

The behavior of orthorhombic distortions for PrCoO_3 and NdCoO_3 is apparently more complex. With increasing temperature they first increase going through a maximum at 230 K and 280 K, respectively, and then decrease. However, this is again in agreement with the dependence of the room temperature lattice parameters on r_{Ln} , as these phases belong to the region with $a > c/\sqrt{2} > b$, *i.e.* where orthorhombic distortion is increasing with r_{Ln} . In the case of NdCoO_3 lattice parameters cross around ≈ 600 K and above this temperature the relation change to $b > c/\sqrt{2} > a$, which is typical for LnCoO_3 with smaller Ln .

The data on linear thermal expansions for LnCoO_3 ($\text{Ln} = \text{Y}, \text{Dy}, \text{Gd}, \text{Sm}, \text{Nd}, \text{Pr}$), completed with LaCoO_3 taken from [5], are displayed in Fig. 4. Thermal expansion coefficients were calculated as an average over the main crystal directions using the formula

$$\alpha(T) = \frac{1}{l_o} \frac{l_2 - l_1}{T_2 - T_1} (K^{-1}) \quad (3)$$

where $l = (V/Z)^{1/3}$, V/Z is the cell volume per formula unit, l_o is the value at room temperature, l_2 and l_1 are values at two close temperatures T_2 and T_1 , and $T = (T_1 + T_2)/2$.

Three essential features could be detected in the thermal expansions of LnCoO_3 : (1) A linear increase of the expansion coefficient α , common within experimental error for all orthorhombic LnCoO_3 , that starts from 100 K and spreads to about 500 K for $\text{Ln} = \text{Y}$ and Dy . (2) A steep enhancement of α due to rapid increase of population of Co^{3+} IS or HS states, that rises from the linear part successively at higher temperatures as Ln radius decreases. In the case of LaCoO_3 this steep enhancement occurs as low as at 35 K (inflection point), so the linear part is missing. Corresponding inflection point temperatures of PrCoO_3 and NdCoO_3 are 230 K and 300 K, respectively. The steep enhancement of the expansion coefficient develops in a maximum clearly visible for LaCoO_3 and PrCoO_3 , but only present

as a shoulder for NdCoO_3 and becoming obscure for still smaller Ln. (3) A broad maximum that shifts with decreasing Ln radius from ≈ 535 K for LaCoO_3 to ≈ 800 K for YCoO_3 . Its height increases from $24 \times 10^{-6}\text{K}^{-1}$ for LaCoO_3 to $42 \times 10^{-6}\text{K}^{-1}$ for GdCoO_3 and then decreases for DyCoO_3 and YCoO_3 .

The broad maximum of thermal expansion at high temperatures can be associated with the I-M transition [4]. This correspondence is also documented by comparison with an apparent activation energy E_A of the electric conduction, shown in the insets of Fig. 4. The same trend in the peak position is observed, only the temperature of the activation energy maximum is 30 - 50 K lower than that of the thermal expansion. This suggests, together with the non-hysteretic character of the transition, that the conducting high-temperature state does not appear suddenly but is preceded by a phase separated mixture where volume fraction of metallic regions grows gradually to beyond percolation. In the case of resistivity, the attainment of percolation is critical, whereas the thermal expansion reflects the bulk.

The phase separated onset of the conducting state in LnCoO_3 is further evidenced by a gradual change of thermoelectric power shown in Fig. 5. The data confirm that the temperature of I-M transition is increasing with decreasing rare-earth ionic radii. The deviation of YCoO_3 from the trend in absolute value of thermoelectric power is probably linked with the Y deficiency ($\text{Y}_{1-y}\text{CoO}_{3-\delta}$) above-mentioned in Experimental section.

Magnetic susceptibility of YCoO_3 and LaCoO_3 is displayed in Fig. 6. Raw susceptibility data contain the main temperature dependent contribution from the excited Co^{3+} states (IS or HS), the paramagnetic Van Vleck susceptibility associated with the field-induced admixture of high-lying levels to the non-magnetic LS Co^{3+} ground state, the diamagnetic contribution of Ln, Co and O core states and, finally, the contribution from paramagnetic impurity which is responsible for the hyperbolic increase of observed susceptibility (Curie-like term) at the lowest temperatures.

The raw data on YCoO_3 suggest that the sum of positive Van Vleck and negative diamagnetic terms is about 10^{-4} emu/mol, which is in agreement with the theoretical prediction of Griffith and Orgel [15] and measurement of NMR shift in spinel Co_3O_4 with LS Co^{3+} in octahedral sites by Kamimura [16]. After the subtraction of such constant value and the above-mentioned impurity term, the corrected susceptibility is directly related to the

number of excited Co^{3+} states $p(T)$ by the expression

$$\chi(T) = \frac{N_A \mu_B^2}{3k_B} \frac{g^2}{T} S(S+1)p(T) \quad (4)$$

supposing, of course, a negligible interaction between excited species. Here, N_A is the Avogadro number, μ_B the Bohr magneton, k_B the Boltzmann constant, g is the Landé factor and S the spin number.

The fit we made to susceptibility data supposed a statistic ensemble of independent Co^{3+} ions with a nonmagnetic (LS) ground state and a magnetic excited state. The population of excited states is then expressed by

$$p(T) = \frac{\nu(2S+1)e^{-\Delta/T}}{1 + \nu(2S+1)e^{-\Delta/T}} \quad (5)$$

where Δ is the energy difference between the ground and excited states in units of T , $2S+1$ and ν are the spin and orbital degeneracies of the excited state (the ground state is the spin and orbital singlet). We used $g = 2$ and $S = 1$, *i.e.* we supposed excited states of the IS character as in the paper of Zobel *et al.* [7]. In distinction to this paper we subtracted more realistic, order of magnitude smaller Van Vleck term and, importantly, allowed for a change of Δ with increasing temperature and IS population. In the calculation we used $\nu = 1$, which presumes that orbital degeneracy is lifted due to local distortions, either static or dynamic. This assumption is necessary for a consistent interpretation of the magnetic and thermal expansion LaCoO_3 data within the LS-IS scenario. For the magnetic transition in YCoO_3 , which is at much higher temperature, the orbital degeneracy might be active, but has little effect for our analysis, except for some renormalization of the $\Delta(T)$ values. Using the calculated $p(T)$ we derived the energy splitting of the ground and excited state as

$$\Delta(T) = T \ln \left[\nu(2S+1) \frac{1 - p(T)}{p(T)} \right] \quad (6)$$

The calculated $p(T)$ and $\Delta(T)$ for YCoO_3 and LaCoO_3 are displayed in Fig. 7. In both cases, $\Delta(T)$ is a decreasing function, which can be related to a combined effect of normal and anomalous lattice expansion, and vanishes at some temperature T_o , corresponding to the LS-IS crossover (see also the electronic structure calculations in [17]). At T_o , where $\Delta(T_o) = 0$, the actual IS/LS ratio is equal to $\nu(2S+1) = 3$. The energy $\Delta(T)$ was arbitrarily fitted by a power function

$$\Delta(T) = E_o \left[1 - \left(\frac{T}{T_o} \right)^n \right] \quad (7)$$

and the dependencies of $\Delta(T)$ on temperature for the other LnCoO_3 systems were estimated simply by a linear interpolation of E_o , T_o and n based on the ionic radii of Ln. The parameters, which are summarized in Table I, were subsequently used for calculation of $p(T)$ curves using Eq. (5).

With the knowledge of $p(T)$ in hand, the model for the thermal expansion of LnCoO_3 can be divided into a three contributions

$$\alpha(T) = \alpha_{latt} + \alpha_{mag} + \alpha_{IM} \quad (8)$$

(1) Lattice term α_{latt} is a weighted sum by $p(T)$ of normal thermal expansions of LnCoO_3 in LS state (α_{LS}) and in excited spin state (α_{IS})

$$\alpha_{latt}(T) = \alpha_{LS}(T)[1 - p(T)] + \alpha_{IS}(T)p(T) \quad (9)$$

(2) The anomalous contribution α_{mag} is related to the temperature change of the amount of excited states, given by a temperature derivative of the Eq. (5)

$$\frac{\partial p}{\partial T} = \frac{\nu(2S + 1)e^{-\Delta/T}}{(1 + \nu(2S + 1)e^{-\Delta/T})^2} \left(\frac{\Delta}{T^2} - \frac{1}{T} \frac{\partial \Delta}{\partial T} \right) \quad (10)$$

and can be expressed as

$$\alpha_{mag}(T) = \frac{\partial p}{\partial T} d_{mag} \quad (11)$$

where $d_{mag} = (l_{IS} - l_{LS})/l_o$.

(3) The contribution α_{IM} refers to the anomalous expansion associated with the I-M transition. For our analysis the α_{IM} term was modelled rather arbitrarily by a gaussian profile

$$\alpha_{IM}(T) = \frac{A_{IM}}{h_{IM}} \sqrt{\frac{4 \ln 2}{\pi}} e^{-4 \ln 2 \left(\frac{T - T_{IM}}{h_{IM}} \right)^2} \quad (12)$$

where A_{IM} is the total area and h_{IM} is the width of the gaussian profile at the half of the maximum.

As concerns the lattice term α_{latt} , we infer from the character of thermal expansion shown for LnCoO_3 in Fig. 4 that the lattice contribution of cobaltite in LS state α_{LS} is linearly increasing at least up to ≈ 400 K. For lattice contribution of cobaltite in IS state α_{IS} we expect a similar trend, by comparing *e.g* with the data for $\text{La}_{0.82}\text{Sr}_{0.18}\text{CoO}_3$ in [7], but with a larger slope, $\alpha_{IS} > \alpha_{LS}$. The expansion coefficients seem to saturate at a value $\alpha_{latt} = 20 \times 10^{-6} \text{K}^{-1}$ at elevated temperatures. At these temperatures IS state should

dominate for all LnCoO_3 systems, so we have chosen $\alpha_{IS} = 20 \times 10^{-6} \text{K}^{-1}$. Somewhat larger experimental value for LaCoO_3 derived from data of Ref. [5] is most likely due to a partial reduction $\text{Co}^{3+} \rightarrow \text{Co}^{2+}$ at high temperatures, caused by the measurement in vacuum. As to the saturated expansion coefficient relevant to the LS state, no direct observation is available. A good fit of the linear part between 100 and 500 K could be obtained with a smaller value $\alpha_{LS} = 14 \times 10^{-6} \text{K}^{-1}$.

The analysis of the anomalous contributions α_{mag} and α_{IM} has been attempted with the aim to derive characteristic parameters d_{mag} and A_{IM} that specify the linear increase of the perovskite cell upon the diamagnetic-paramagnetic and I-M transitions, respectively. The best fit has been obtained with $d = 0.35\%$ and $A_{IM} = 0.32\%$ (volume change in both cases about 1%).

The temperature positions of maxima T_{mag} and T_{IM} of the α_{mag} and α_{IM} contributions, respectively, are found to increase linearly with decreasing Ln radius (see Table I). The width of the gaussian profile of α_{IM} remains practically constant, $h_{IM} \sim 225$ K. The fit curves of thermal expansions for all LnCoO_3 are displayed in Fig. 4. Examples of the fit of thermal expansion and the 3 contributions for PrCoO_3 , SmCoO_3 and YCoO_3 are displayed in Fig. 8.

Our value d_{mag} is smaller than $d = 0.66\%$ reported previously for LaCoO_3 by Zobel *et al.* in [7] on the basis of their dilatometric measurements. This difference has two origins. First, the present expansion data for LaCoO_3 deduced from neutron diffraction [5] are about $1.5 \times$ lower than the dilatometric data. Second difference is that they supposed constant energy splitting Δ whereas we allow decrease of Δ with temperature.

Although we denote the second transition as insulator-metal, it is evidently connected for all LnCoO_3 with some kind of magnetic transition, which was, however, so far only evidenced for LaCoO_3 . The insulator-metal transition itself should not be accompanied by a positive contribution to thermal expansion. From the similar shape of both contributions (see Fig. 8) we infer, that the origin of the second transition also lies in the thermal excitations to another paramagnetic state separated by energy splitting which vanishes with temperature.

IV. CONCLUSION

The X-ray diffraction study was performed on a series of LnCoO_3 perovskites ($\text{Ln} = \text{Y}$, Dy , Gd , Sm , Nd , Pr and La) over a broad range of temperatures up to 1000 K. Structural effects associated with the spin-state transitions of Co^{3+} ions, in particular the anomalous thermal expansion, were analyzed in combination with electric transport measurements and, for $\text{Ln} = \text{Y}$ and La , with the magnetic susceptibility data. As a result, the temperature dependence of linear expansion coefficients of LnCoO_3 was fitted using a small number of parameters which are either constant - d_{mag} and A_{IM} - or depend linearly on the Ln ionic radius - E_o , T_o and T_{IM} . The observed expansion is a sum of three contributions:

1. Weighted sum of the lattice expansions of cobaltite in the diamagnetic LS state and in the paramagnetic IS or HS state.
2. The anomalous contribution due to the increasing population of excited IS or HS states at the course of the diamagnetic-paramagnetic transition.
3. The anomalous contribution due to the I-M transition associated with excitations to another paramagnetic state.

The analysis shows that the volume change during two successive magnetic and electronic transitions is independent on the kind of Ln cation and, interestingly, it is of similar amplitude in both cases, namely 1%. In a linear dimension, this volume increase corresponds to a change of the Co^{3+} ionic radius from 0.545 Å for LS state to 0.552 Å and 0.558 Å after the diamagnetic-paramagnetic and I-M transitions, respectively. This change is too small to be compared with radius of Co^{3+} ion in HS state ($r_{HS} = 0.61$ Å). The expansion data are thus in favor of the IS ($r_{IS} = 0.56$ Å) nature of magnetic Co^{3+} species in LnCoO_3 .

Within such LS-IS scenario, the present model calculations provide the values of the LS-IS gap and their evolution with temperature, and allow to estimate the temperature rate of IS population during the magnetic transition in LnCoO_3 compounds where investigation of the Co^{3+} magnetism is hindered due to a much larger rare-earth contribution.

Acknowledgments

The work was supported in part by the European Community's Human Potential Programme under contract HPRN-CT-2002-00293, SCOOTMO.

- [1] J. Hejtmánek, Z. Jirák, K. Knížek, M. Maryško, M. Veverka, and H. Fujishiro, *J. Magn. Magn. Mat.* **272-276**, E283 (2004).
- [2] J.-Q. Yan, J.-S. Zhou, and J. B. Goodenough, *Phys. Rev. B* **69**, 134409 (2004).
- [3] L. Sudheendra, M. M. Seikh, A. R. Raju, and C. Narayana, *Chem. Phys. Lett.* **340**, 275 (2001).
- [4] S. Yamaguchi, Y. Okimoto, and Y. Tokura, *Phys. Rev. B* **54**, R11022 (1996).
- [5] P. G. Radaelli and S.-W. Cheong, *Phys. Rev. B* **66**, 094408 (2002).
- [6] G. Maris, Y. Ren, V. Volotchaev, C. Zobel, T. Lorenz, and T. T. M. Palstra, *Phys. Rev. B* **67**, 224423 (2003).
- [7] C. Zobel, M. Kriener, D. Bruns, J. Baier, M. Grüninger, T. Lorenz, P. Reutler, and A. Revcolevschi, *Phys. Rev. B* **66**, R020402 (2002).
- [8] K. Asai, O. Yokokura, N. Nishimori, H. Chou, J. M. Tranquada, G. Shirane, S. Higuchi, Y. Okajima, and K. Kohn, *Phys. Rev. B* **50**, 3025 (1994).
- [9] K. Asai, A. Yoneda, O. Yokokura, J. M. Tranquada, G. Shirane, and K. Kohn, *J. Phys. Soc. Japan* **67**, 290 (1998).
- [10] X. Liu and C. Prewitt, *J. Phys. Chem. Solids* **52**, 441 (1991).
- [11] G. Demazeau, M. Pouchard, and P. Hagenmuller, *J. Solid State Chem* **9**, 202 (1974).
- [12] A. Mehta, R. Berliner, and R. Smith, *J. Solid State Chem* **130**, 192 (1997).
- [13] J.-Q. Yan, J.-S. Zhou, and J. B. Goodenough, *Phys. Rev. B* **70**, 014402 (2004).
- [14] *Inorganic Crystal Structure Database. National Institute of Standards and Technology (NIST) and Fachinformationszentrum Karlsruhe (FIZ)* (version 2004).
- [15] J. S. Griffith and L. E. Orgel, *Trans. Faraday Soc.* **53**, 601 (1957).
- [16] H. Kamimura, *J. Phys. Soc. Japan* **21**, 484 (1966).
- [17] M. A. Korotin, S. Y. Ezhov, I. V. Solovyev, V. I. Anisimov, D. I. Khomskii, and G. A. Sawatzky, *Phys. Rev. B* **54**, 5309 (1996).

TABLE I: Ionic radii r_{Ln} for 9-fold coordination and the fit parameters of the analysis of magnetic and structural data of LnCoO_3 : Energy splitting E_o of the ground and excited state at $T = 0$ K, temperature of LS-IS crossover T_o and power coefficient n , see Eq. (7). The temperature positions of maxima T_{mag} and T_{IM} of the α_{mag} and α_{IM} contributions, respectively.

	r_{Ln}	E_o	T_o	n	T_{mag}	T_{IM}
	(Å)	(K)	(K)		(K)	(K)
YCoO_3	1.075	2875	860	3.51	780	800
DyCoO_3	1.083	2721	825	3.48	740	785
GdCoO_3	1.107	2260	717	3.39	619	740
SmCoO_3	1.132	1779	605	3.29	493	693
NdCoO_3	1.163	1183	466	3.17	337	635
PrCoO_3	1.179	875	395	3.11	256	605
LaCoO_3	1.216	164	230	2.97	70	535

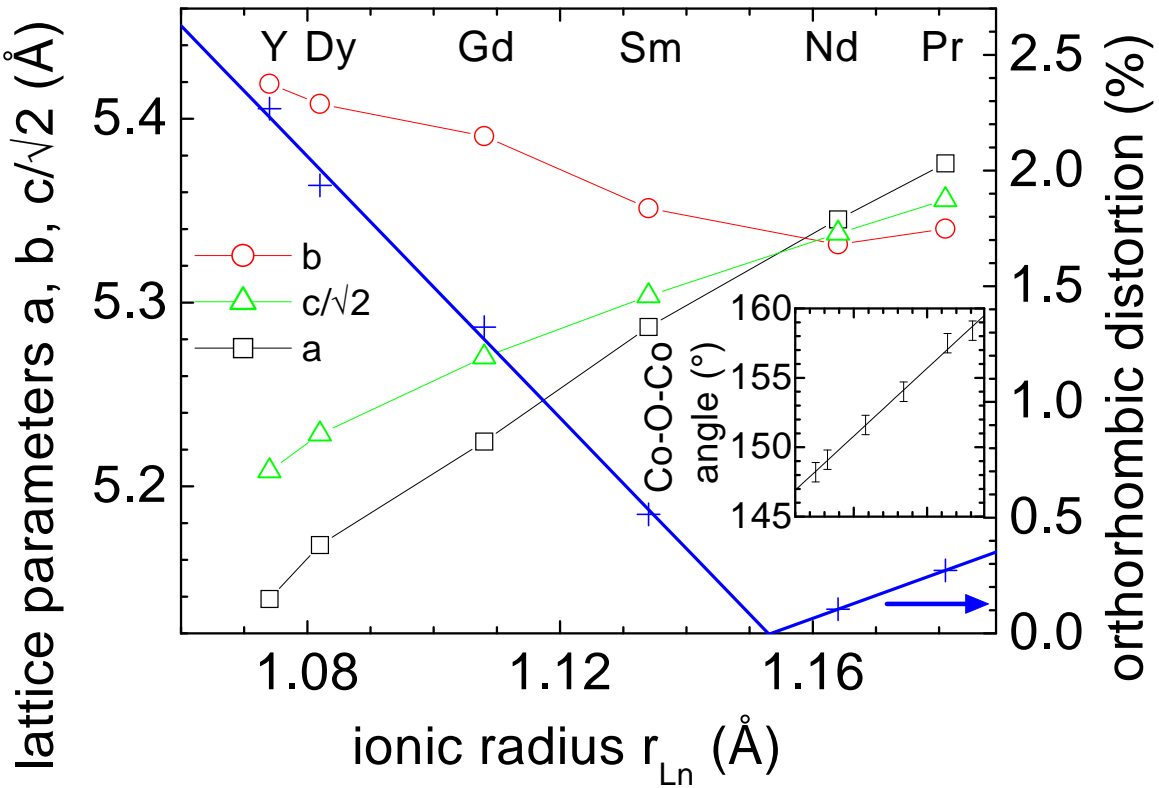


FIG. 1: Lattice parameters and orthorhombic distortion (Eq. (2)) *vs.* Ln ionic radius for LnCoO_3 (Ln = Y, Dy, Gd, Sm, Nd and Pr) at room temperature. All structures were refined within the $Pbnm$ space group. The inset shows the average Co-O-Co bond angle. The scale of the x-axis of the inset is omitted and is identical with that of the main figure.

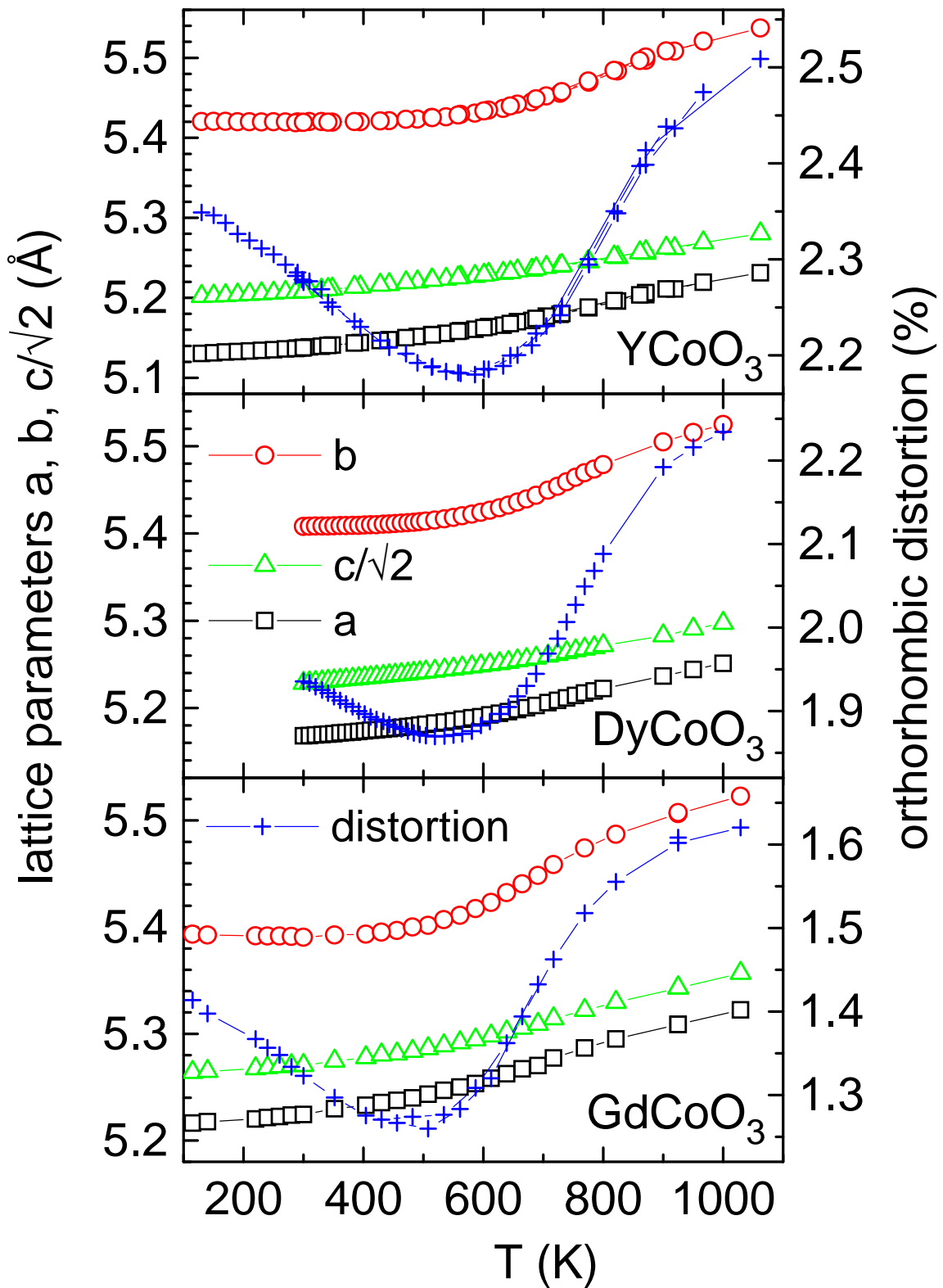


FIG. 2: Lattice parameters and orthorhombic distortion (Eq. (2)) *vs.* temperature for YCoO_3 , DyCoO_3 and GdCoO_3 .

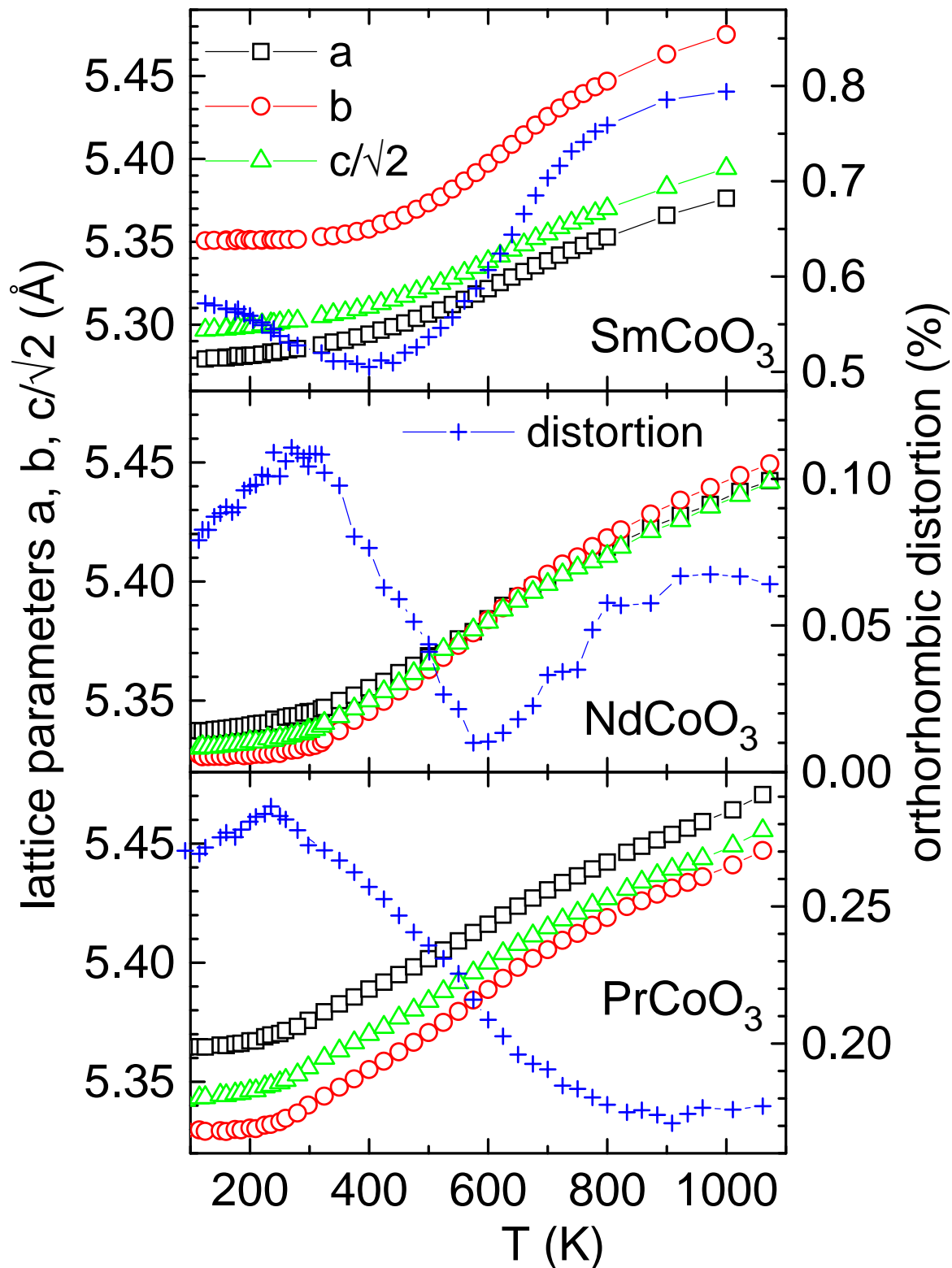


FIG. 3: Lattice parameters and orthorhombic distortion (Eq. (2)) *vs.* temperature for SmCoO_3 , PrCoO_3 and NdCoO_3 .

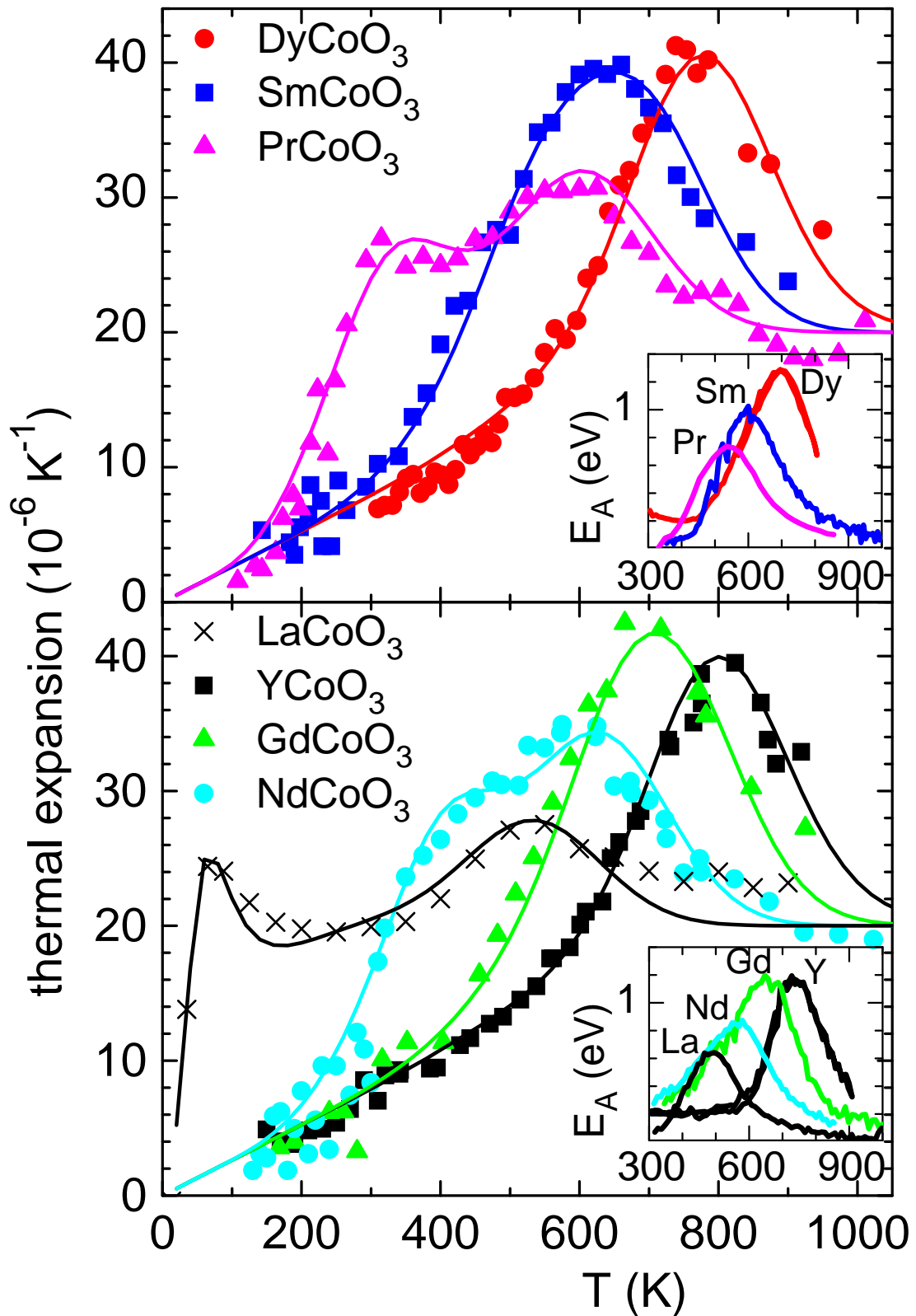


FIG. 4: Linear thermal expansion α (Eq. (3)) for LnCoO_3 and LaCoO_3 [5]. The solid lines are calculated fits of α . The inset shows apparent activation energy $E_A = d \ln \rho / d(T^{-1})$ calculated from resistivity ρ .

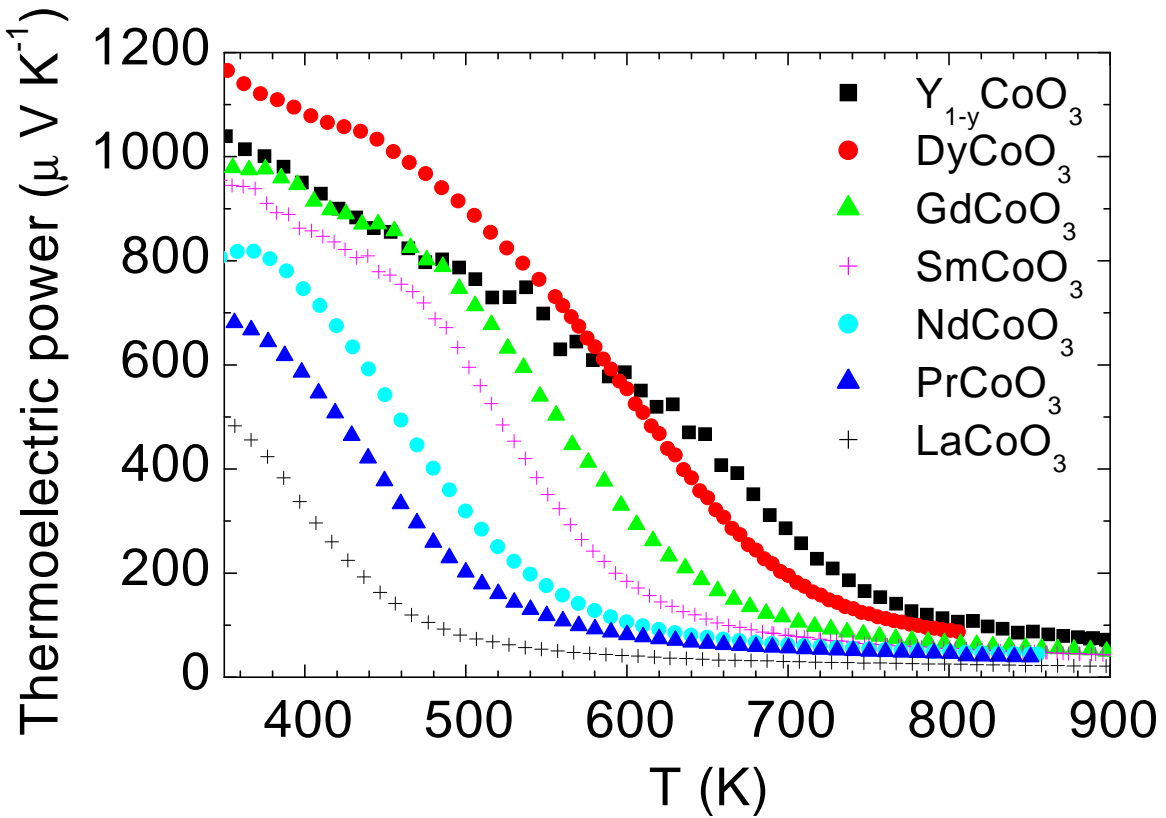


FIG. 5: High temperature thermoelectric power of LnCoO_3 .

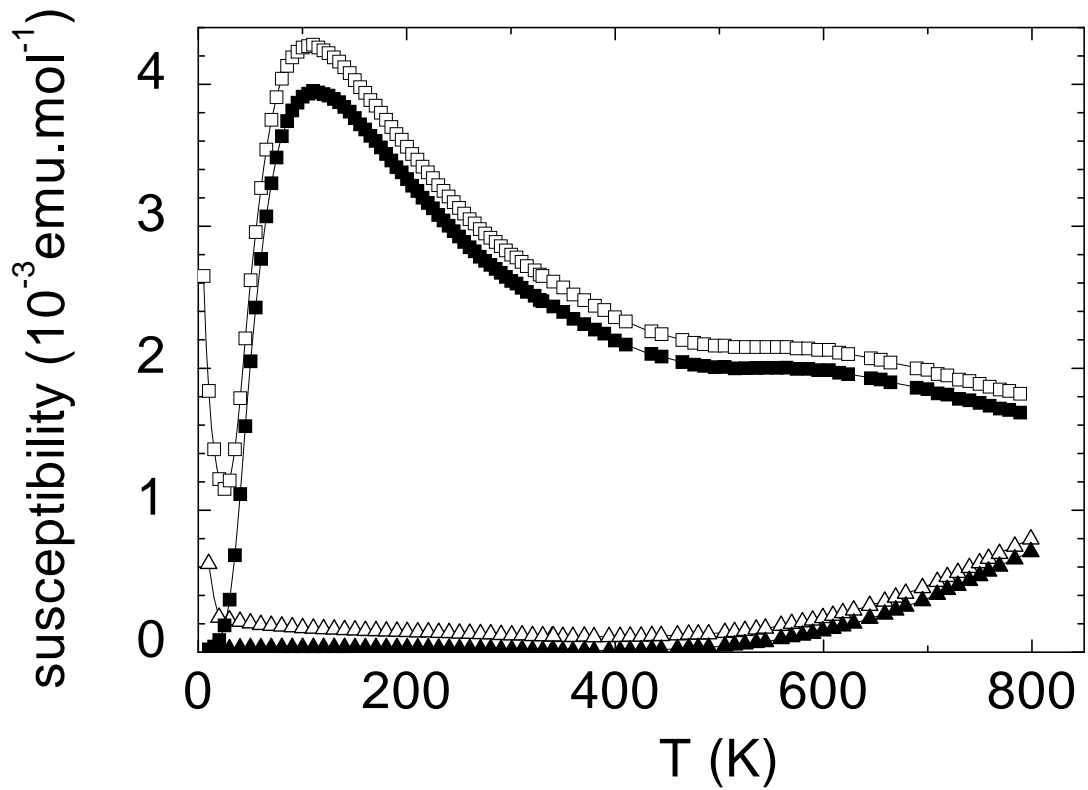


FIG. 6: Magnetic susceptibility of YCoO₃ (\triangle) and LaCoO₃ (\square). Raw data are displayed in open symbols, corrected data in full symbols.

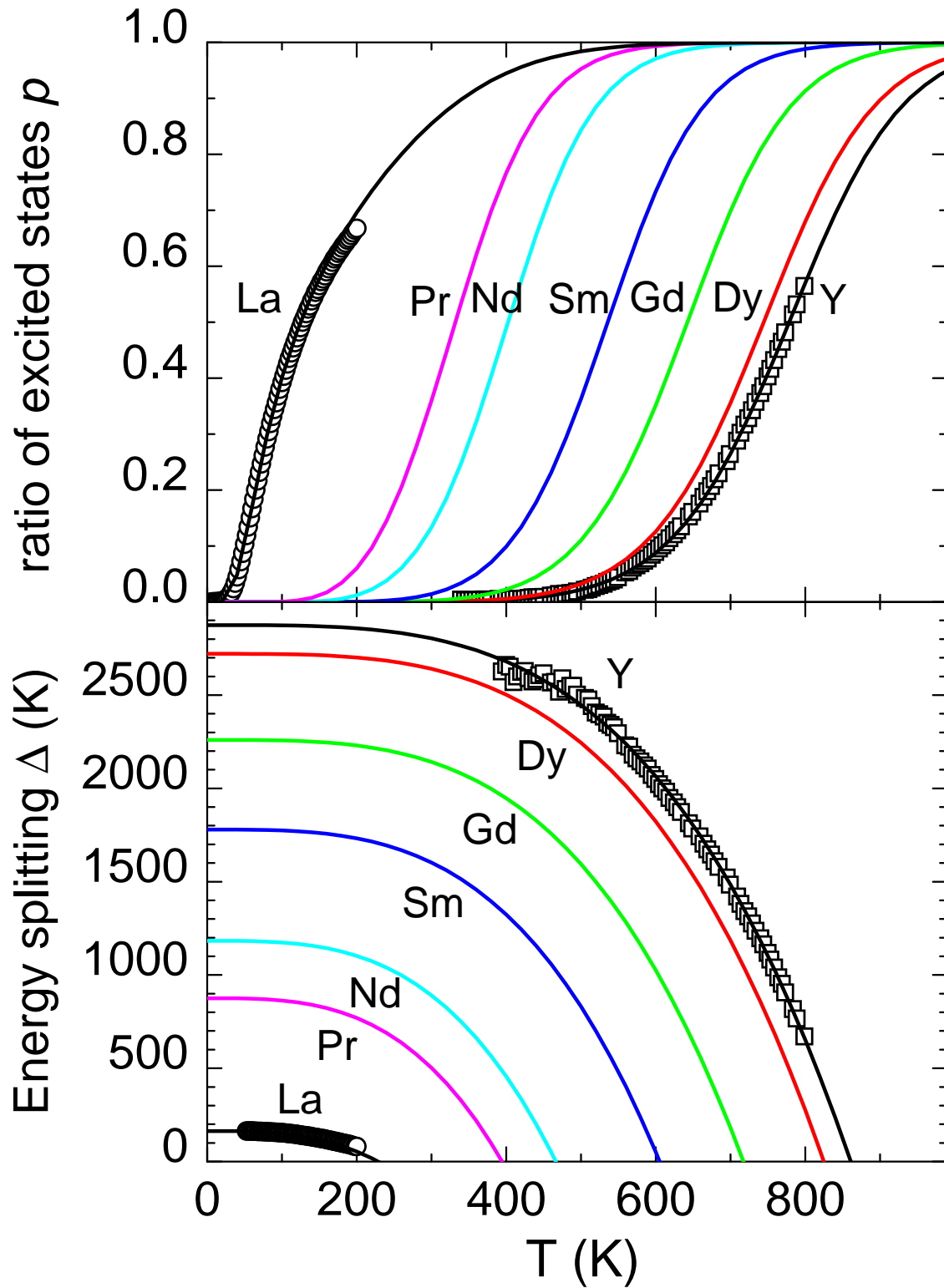


FIG. 7: Ratio of excited states p and energy splitting between ground and excited spin states Δ calculated from magnetic susceptibility for YCoO_3 and LaCoO_3 and interpolated for the other
 21 LnCoO_3 .

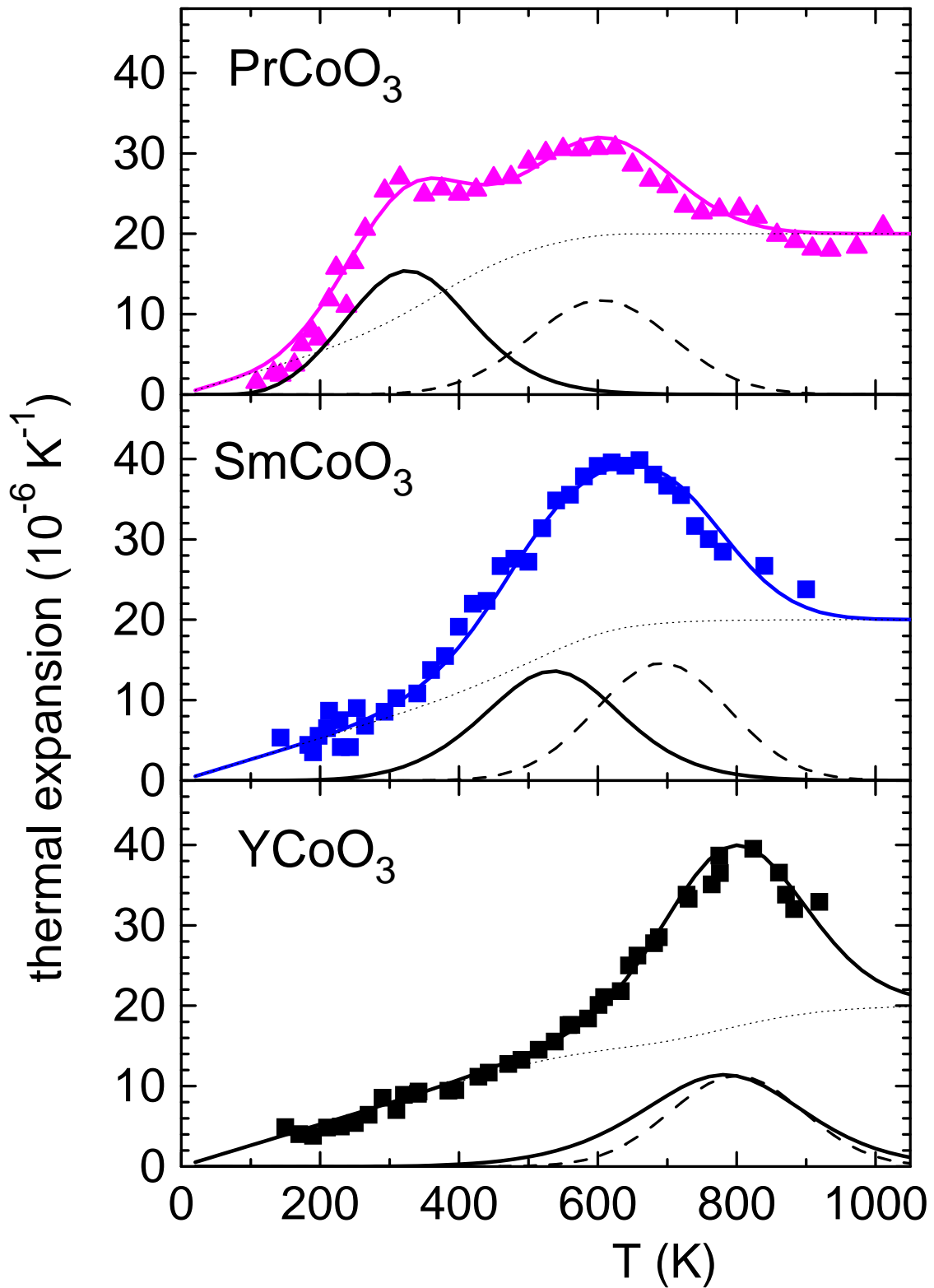


FIG. 8: Examples of the fits of thermal expansion and the three contributions α_{latt} (\cdots), α_{mag} ($-$) and α_{IM} ($-\cdot-$) for PrCoO_3 , SmCoO_3 and YCoO_3 .